Raman signatures of novel electronic states in BCT lattice

Carlene Paula Silva de Farias, Sebastien Burdin, Alvaro Ferraz

Raman signatures of novel electronic states in BCT lattice

Carlene Silva de Farias,[1,2,*] Sébastien Burdin,[1,†] and Alvaro Ferraz.[2]

[1] *Université Bordeaux, CNRS, LOMA, UMR 5798, F 33400 Talence, France*
[2] *Departamento de Física Teórica e Experimental and International Institute of Physics, Universidade Federal do Rio Grande do Norte, Natal, Brasil.*

(Dated: October 26, 2017)

We propose an effective model to describe the Raman scattering experiments in crystalline materials with body-centered tetragonal (BCT) lattice. Our model takes into account different emerging spin liquid states. The states display the breaking of lattice translation symmetry from a body-centered tetragonal (BCT) to simple tetragonal (ST). The breaking of lattice translation symmetry results in a folding of the Brillouin zone, which translates itself into either a gap or a pseudogap. This (pseudo) gap can be observed in the Raman spectra for each of the irreducible symmetries that we investigate. We introduce an alternative approach to the effective mass approximation to treat the A_{2g} symmetry based on resonant process. The results for the A_{2g} symmetry show that there is a Raman response associated with a particular spin liquid phase which also produces a gap if we include modulation effects linked to a specific local staggered order. We also discuss the relevance of this result for the problem of hidden order in URu_2Si_2 and to the A_{2g} results referred by recent experiments. Complementing these analysis, we use the standard effective mass approximation to analyze the responses associated with each state for the A_{1g}, B_{1g} and B_{2g} irreducible symmetries.

PACS numbers: 71.27.+a, 78.30.-j, 75.10.Kt

I. INTRODUCTION

Raman spectroscopy has become an indispensable experimental tool for understanding the physics of strongly correlated systems. It has been used to characterize excitations in cuprates [1–3], iron-based superconductors [4, 5], heavy fermions [6–8] and more recently in systems that exhibit elementary excitations with a topological character [9, 10]. This experimental technique can provide a wealth of quantitative and qualitative information about the electronic behavior and the lattice dynamics of systems [11]. It also contains information about the unconventional charge and spin dynamics, such as the possible existence of unconventional "chiral" spin state and charge currents [12, 13].

In this article, we present an effective theory to model Raman scattering experiments of new ordered states in a body-centered tetragonal (BCT) lattice. Similar effective models were proposed with the purpose of investigating the hidden order phase in URu_2Si_2 [14–16]. In a general manner, this paper makes use of our previous work [17], where we have demonstrated the possibility of stabilizing both the Antiferromagnetic (AF) and the spin liquid (SL) phases in this particular lattice structure. The phase diagram shows the competition between these two phases by the variation of one parameter that characterizes either the spin or the orbital degeneracy. Here we shall consider the interplay between different spin liquid states. With the aim of applying the symmetry analysis of Harima *et al.* [18] to that Raman data, we shall relate each phase with a particular space (point) group that will be introduced by means of a specific parameter. Each of these states break the lattice translation symmetry from BCT to simple tetragonal (ST) which translates into distinct Raman signatures that are related to different parameters present in our model.

In the case of the space group No 139 (D_{4h} point group), associated with the fully symmetric BCT lattice, the polarization of the incident and the scattered light set in the experiment maps the excitation modes associated with the irreducible representations of the crystal structure. We shall focus in the A_{1g}, A_{2g}, B_{1g} B_{2g} symmetries. A standard approach that one can use to simplify the analysis is the effective mass approximation, which assumes that there is no transference of momentum between the experimental setup and the sample. As a consequence of that, the "effective density" measured by Raman is weighted by a factor which is proportional to linear combinations of the second derivative of the dispersion of the system with respect to the components of momentum. However, this assumption cannot provide any signal in A_{2g}. Thus, we introduce an alternative approach for A_{2g}, that takes into account the resonant effects of the scattering process.

The outline of the paper is as follows. In section II we present our effective model. We introduce the effective Hamiltonian with the specific parameters that take into account the possible phases associated with each space group. In section III, we describe how we can obtain the signal for the A_{2g} symmetry and show our numerical results for it. We also discuss the connection between the real experimental finding for URu_2Si_2 in this particular symmetry and the possible spin liquid scenarios. In section IV, we shall describe our theoretical approach and numerical results for the Raman response for the A_{1g}, B_{1g}

* cfarias@ifi.unicamp.br
† sebastien.burdin@u-bordeaux.fr

and B_{2g} symmetries. In section V, we discuss our most significant results and their relation to other experiments. Finally, soon after that we present our conclusion.

II. THE MODEL

A crucial ingredient to build an effective model is the underlying lattice symmetry that we want to address. Here, we propose a Hamiltonian that describes spinless fermions that are moving throughout the sites of a BCT lattice by means of a kinetic hopping term. This effective phenomenological model can emerge from a realistic microscopic approach when correlations stabilize SL states [17, 19] or any other commensurate state with a folded Fermi surface, like e.g., the orbital density waves [14], Fermi surface instability [15] or spin-density waves [16]. In this work, we do not consider further effects of fluctuations on top of those correlated effects. Instead, we focus on low energy Fermi liquid-like excitations of these states with the specific BCT lattice broken symmetry.

We can write down the Hamiltonian as

$$H = \sum_i (E_0 + m e^{i\mathbf{Q}\cdot\mathbf{R}_i}) c_i^\dagger c_i + \sum_{\langle i,j\rangle} t_{ij} c_i^\dagger c_j \qquad (1)$$

The operators $c_i^\dagger$ and c_i represent the creation and annihilation of spinless fermions at a given site i with position $\mathbf{R}_i$. The parameter E_0 adjusts the chemical potential while m defines a commensurate local staggered order (LSO). The hopping t_{ij} connects nearest neighbors on the BCT lattice, but, besides that, it may also break the BCT symmetry down to the ST lattice symmetry.

In the Paramagnetic (PM) phase, the lattice structure is BCT symmetric. We assume that the system suffers a phase transition to a particular state with a lower lattice symmetry, namely the simple tetragonal (ST). This lowering of symmetry is characterized by a folding in the Brillouin zone (BZ) from the BCT lattice into the ST one. The Z and Γ points of the first BZ of the ST and BCT, respectively, are connected by the nesting vector $\mathbf{Q} = \{1, 1, 1\}$.

The possible states we consider are represented in Fig.1. Their relation with the point group symmetries (space group) and the model parameters is summarized in table I. We start in the framework of a normal PM state with the system having its structure defined by the BCT space group No 139 ($I4/mmm$, D_{4h}). We assume that it can pass from this normal state to a new phase defined with three different ST space groups which could be associated with the No 123 ($P4/mmm$, D_{4h}), the No 126 ($P4/nnc$, D_4) or the No 128 ($P4/mnc$, C_{4h}). Moreover, the point groups D_4 and C_{4h} have the same selection rules in a Raman experiment as the initial point group D_{4h} [18].

We introduce appropriate parameters that capture the space groups of the different ordered states. As we mention previously, the parameter $me^{i\mathbf{Q}\cdot\mathbf{R}_i}$ can account for some commensurate local staggered order (LSO) with local (onsite) order parameters. The space group No 128 ($P4/mnc$) characterizes a chiral spin liquid (CSL) phase with complex nearest neighbors hopping parameter $t_{ij} = t_1 \pm i\Delta_c$. The space group No 126 ($P4/nnc$)

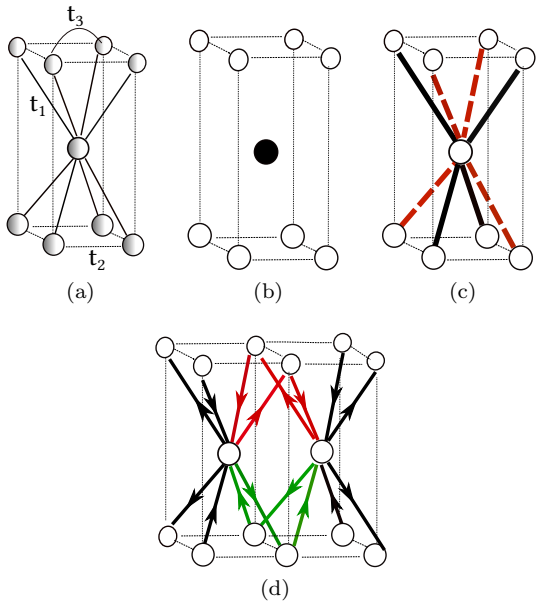

FIG. 1. Schematic representation of the four possible ordered states that we consider in our model. Figure (**a**) shows the paramagnetic phase that displays the full BCT lattice structure with space group No 139. Figure (**b**), displays the Antiferromagnetic state, which has the simple tetragonal lattice, with space group symmetry No 123.In (**c**), we represent the modulated SL phase, associated with the space group No 126. In (**d**), we display the chiral SL phase, that is related to the space group No 128.

TABLE I. Summary of the point groups and phases that specify each of them. We determine whether the point groups break or not the symmetries of D_{4h}. The operations are Time-reversal symmetry ($\mathcal{TR}$), inversion symmetry ($\mathcal{I}$), rotations of $\pi/2$ (C_4) and reflections related to xy plane.

Label in Fig.(1)	(a)	(b)	(c)	(d)
Phase	PM	LSO	MSL	CSL
Space group	No 139 ($I4/mmm$) D_{4h}	No 123 ($P4/mmm$) D_{4h}	No 126 ($P4/nnc$) D_4	No 128 ($P4/nmc$) C_{4h}
Model parameters	$m = 0$, $\Delta_m = 0$, $\Delta_c = 0$	$m \neq 0$, $\Delta_m = 0$, $\Delta_c = 0$	$m = 0$ or $m \neq 0$, $\Delta_m \neq 0$, $\Delta_c = 0$	$m = 0$ or $m \neq 0$, $\Delta_m = 0$, $\Delta_c \neq 0$
Lattice structure	BCT	ST	ST	ST
$\mathcal{TR}$	✓	✓	✓	x
$\mathcal{I}$	✓	✓	x	✓
$\mathcal{C}_4$	✓	✓	x	x
$\mathcal{P}_{xy}$	✓	✓	x	✓

characterizes a modulated spin liquid (MSL) phase with a real nearest neighbor hopping $t_{ij} = t_1 \pm \Delta_M$. In this definitions, m, Δ_c and Δ_m are real positive quantities.

Since the c's operators represent fermions, the magnetic state, specified by the parameter m, is justified by the fact that the fermions here are like spinons in a deconfined phase which have an intrinsic magnetic moment. They lead to the formation of SL phases and represent the elementary excitations of the system, which possess the general character of being fractionalized [20].

If the hopping parameter t_{ij} is complex, its imaginary part is associated with the parameter Δ_c. The sign choice in the definitions of t_{ij} relates itself to the orientation of the link between two neighboring sites at different planes. In approaching a site, we consider the plus sign, and if the link leaves the site, we choose the minus sign (see Fig.1(d)) instead. If t_{ij} is real, we add the term Δ_m to the hopping between the first neighbors at different planes, that is associated with the MSL phase, which is schematically illustrated in Fig.1(c). The choice of the plus or minus sign if t_{ij} is real represents the kind of bond between the first neighbors at different planes. The other real cases are $t_{ij} = t_2$ for first neighbors in-plane and $t_{ij} = t_3$, for the second neighbors in-plane, see Fig.1(a). Indeed, in this work, for the sake of clarity, we do not investigate the possibility of the in-plane ordering that might be associated with different lattice symmetry breaking.

By using the Fourier decomposition of the c_i operator

$$c_i = \frac{1}{\sqrt{N}} \sum_{\mathbf{k}} e^{i\mathbf{k}\cdot\mathbf{R}_i} c_{\mathbf{k}}, \tag{2}$$

where the sum in $\mathbf{k}$ runs over the first Brillouin zone of the BCT lattice, we write down the Hamiltonian in matrix representation with a folded Brillouin zone from the BCT to the ST (see appendix A). The Hamiltonian in second quantized form becomes

$$\hat{H} = \sum_{\mathbf{k}} \Psi^{\dagger}_{\mathbf{k}} h_{\mathbf{k}} \Psi_{\mathbf{k}}, \tag{3}$$

with the sum over $\mathbf{k}$ now running over the first Brillouin zone of the ST lattice (see a more detailed calculation in Appendix A). Using the definition of the two-component spinor $\Psi_{\mathbf{k}} = (c_{\mathbf{k}}, c_{\mathbf{k}+\mathbf{Q}})^t$, it follows that

$$h_{\mathbf{k}} = \begin{pmatrix} \varepsilon_{\mathbf{k}} & V^*_{\mathbf{k}} \\ V_{\mathbf{k}} & \varepsilon_{\mathbf{k}+\mathbf{Q}} \end{pmatrix}, \tag{4}$$

where $\varepsilon_{\mathbf{k}} = E_0 + t_1\gamma^1_{\mathbf{k}} + t_2\gamma^2_{\mathbf{k}} + t_3\gamma^3_{\mathbf{k}}$ and $V_{\mathbf{k}} = m + i\Delta_{SL} f_{SL}(\mathbf{k})$. Δ_{SL} can either be Δ_m or Δ_c if we choose the space group to be that of either a modulated or chiral spin liquid, respectively. $f_{SL}(\mathbf{k})$ is defined as

$$f_c(\mathbf{k}) = 8\sin\left(\frac{k_x a}{2}\right)\sin\left(\frac{k_y a}{2}\right)\cos\left(\frac{k_z c}{2}\right), \tag{5}$$

$$f_m(\mathbf{k}) = 8\sin\left(\frac{k_x a}{2}\right)\sin\left(\frac{k_y a}{2}\right)\sin\left(\frac{k_z c}{2}\right), \tag{6}$$

The derivation of the γ's factors is made in the appendix A. The off-diagonal term $V_{\mathbf{k}}$ couples the two bands which are connected to each other by a nesting wave vector $\mathbf{Q}$. The structure factors are defined as

$$\gamma^1_{\mathbf{k}} = 8\cos\left(\frac{k_x a}{2}\right)\cos\left(\frac{k_y a}{2}\right)\cos\left(\frac{k_z c}{2}\right), \tag{7}$$

$$\gamma^2_{\mathbf{k}} = 2(\cos(k_x a) + \cos(k_y a)), \tag{8}$$

$$\gamma^3_{\mathbf{k}} = 4\cos(k_x a)\cos(k_y a), \tag{9}$$

where a and c are the ST lattice constants.

The symmetry operations which we address in our model are respectively the time-reversal ($\mathcal{TR}$) symmetry, the inversion symmetry $\mathcal{I}$, the four-fold rotational symmetry C_4 $(\pi/2)$ and the two reflection symmetries concerning the planes $\mathcal{P}_{x/y}$. The $\mathcal{TR}$ invariance requires that $V_{\mathbf{k}} = V^*_{-\mathbf{k}}$, which is the case for the modulated SL while for the chiral SL case, we must break the time-reversal symmetry. Concerning the C_4 $(\pi/2)$ rotations, the modulated and chiral spin liquid break that rotational symmetry. The MSL phase breaks the reflection symmetry concerning the plane $\mathcal{P}_{xy}$ while CSL preserves it.

The diagonalization of the effective Hamiltonian defined by Eq.(3) and Eq.(4) gives the following dispersion bands

$$E^{\pm}_{\mathbf{k}} = \frac{\varepsilon_{\mathbf{k}} + \varepsilon_{\mathbf{k}+\mathbf{Q}}}{2} \pm \sqrt{|V_{\mathbf{k}}|^2 + \left(\frac{\varepsilon_{\mathbf{k}} - \varepsilon_{\mathbf{k}+\mathbf{Q}}}{2}\right)^2}. \tag{10}$$

This dispersion is defined precisely in the ST Brillouin zone that results from the folding of the BCT Brillouin zone. When computing the correlation function, we have to take into account the dispersion of these two bands.

In the space group No 139, depending on the polarization of the incident and of the scattered lights, we can decompose the excitation modes into six irreducible representations of the D_{4h} point group. They are the A_{1g}, A_{2g}, B_{1g}, B_{2g} and two modes E_g. Our focus will be on the A_{2g} symmetry. Since the effective mass approximation, which is mostly used to analyze the Raman scattering is not able to produce any signal for the A_{2g}, we present an alternative approach to studying this particular symmetry based on resonant scattering [12]. Later on, we may complement our analysis by computing the responses in other symmetries, like A_{1g},B_{1g} and B_{2g}, by using the effective mass approximation, that we know can produce a signal in Raman scattering in these symmetries. Our calculation take as the Raman response the contribution of the imaginary part of the correlation function, which might be defined in terms of a effective density or current operator (resonant process). The response is weighted by a respective vertex, which is associated with the irreducible symmetry under investigation.

III. THE A_{2g} SYMMETRY

As we have mentioned in the end of in the previous section that the effective mass approximation is not able to produce any response in the A_{2g} symmetry. The interesting feature about A_{2g} is that it is usually associated with excitations that possess a chiral nature, as it was pointed out to be the case for Mott insulators used to describe the high-T_c cuprates systems [1, 12].

In this context, for example, the denomination "Magnetic Raman scattering" refers to the scattering by the spin degrees of freedom which are associated with the fluctuations of a chiral operator [1, 12]. This type of scattering is dominated by resonant contributions, which are produced by the current operator instead of the effective density correlation function [2]. In order to obtain signatures of this particular symmetry, we have to consider a different correlation function, which in our context will play the role of a resonant scattering.

We define an operator that, in the framework of our effective non-interacting model, is essentially the current-current commutator at equal time,

$$\hat{M}_{\mu\nu}(\mathbf{q},\tau) = [\hat{j}_\mu(\mathbf{q},\tau), \hat{j}_\nu(\mathbf{q},\tau)], \tag{11}$$

with the current operator being defined as

$$\hat{j}_\mu(\mathbf{q},\tau) = \sum_{\mathbf{k}} \Psi^\dagger_{\mathbf{k}+\mathbf{q}/2}(\tau)\tilde{\boldsymbol{\gamma}}^\mu_R(\mathbf{k})\Psi_{\mathbf{k}-\mathbf{q}/2}(\tau), \tag{12}$$

where $\tilde{\boldsymbol{\gamma}}^\mu_R(\mathbf{k})$ is the matrix which originate from the derivatives of $h_\mathbf{k}$ with respect to the component k_μ. The index R in the vertex is a symbol for resonant contribution. We can extract the signal for A_{2g} by computing the following correlation function

$$\tilde{\chi}^{A_{2g}}(\mathbf{q}, i\omega_n) = -\frac{1}{\mathcal{V}}\int_0^\beta d\tau\, e^{i\omega_n\tau}\langle T_\tau \hat{M}^{A_{2g}}(\mathbf{q},\tau)\hat{M}^{A_{2g}}(-\mathbf{q},0)\rangle. \tag{13}$$

The T_τ is the time-ordering operator, $\mathcal{V}$ is the volume of the Brillouin zone, and the operator $\hat{M}^{A_{2g}}(\mathbf{q},\tau) = \hat{M}_{xy}(\mathbf{q},\tau) - \hat{M}_{yx}(\mathbf{q},\tau)$. At this point we can make $\mathbf{q}\to 0$ without loss of generality, and then, we find that

$$\tilde{\chi}^{A_{2g}}(i\omega_n) = \frac{1}{\beta\mathcal{V}}\sum_{\mathbf{k},n}\mathrm{Tr}\left[\tilde{\gamma}^{A_{2g}}_R(\mathbf{k})G_\mathbf{k}(i\nu_{n'}+i\omega_n)\tilde{\gamma}^{A_{2g}}_R(\mathbf{k})G_\mathbf{k}(i\nu_{n'})\right]. \tag{14}$$

We use the finite temperature representation of the Green's function, where β is the usual inverse of the temperature $1/k_BT$ and $\omega_n = 2n\pi/\beta$ is a bosonic Matsubara frequency. The imaginary part is obtained by performing the analytical continuation in the frequency domain $i\omega_n \to \omega + i\delta$, with δ being a small scattering rate. The Green's functions $G_\mathbf{k}$ can be expressed directly in terms of the elements in their eigenbasis, i.e. $G^\pm_\mathbf{k}(i\nu_{n'}) = 1/(i\nu_{n'} - E^\pm_\mathbf{k})$, by invoking the $E_\mathbf{k}$ eigenvalues in Eq.(10), with $\nu_{n'} = (2n+1)\pi/\beta$ being the fermionic Matsubara frequency. Notice that we can define a different vertex for that A_{2g} symmetry, that differs from the one coming from the effective mass approximation (see next section), that now happens to be defined as

$$\tilde{\gamma}^{A_{2g}}_R(\mathbf{k}) = \frac{\partial h_\mathbf{k}}{\partial k_x}\frac{\partial h_\mathbf{k}}{\partial k_y} - \frac{\partial h_\mathbf{k}}{\partial k_y}\frac{\partial h_\mathbf{k}}{\partial k_x}. \tag{15}$$

This vertex definition resembles the commutation relation between the first derivatives of $h_\mathbf{k}$ with respect to the components k_x and k_y. It is nonzero if we take the derivatives of Eq.(4) and it represent the vertex that could be associated with a Resonant process. Regarding that a resonant Raman process must have a fourth order vertex, our correlation function in Eq.(14) satisfy this requirement. In the Appendix B, we explain how we can extract the A_{2g} response in terms of a matrix algebra by making use of the direct Pauli matrices.

Proceeding with the numerical analysis, we compute the correlation function for A_{2g} in Eq.(14). We take the $T\to 0$ limit and keep t_1 activated. The plots in Fig.2 represent the results for the A_{2g} symmetry at the modulated and chiral SL phases. Whereas in Fig.3 we display the feature of the Raman response in the presence of the m parameter.

In Figs.2(**a**)-(**b**), we vary the values of parameters for the spin liquids. The space groups for each of these figures are the Nos 126 and 128, respectively. By increasing the values of Δ_m or Δ_c, in both cases, we observe the enhancement of the signal by increasing the values of Δ_m or Δ_c. The lineshape for both phases are similar assuming a Drude response. No gap is observed for both states.

We also verify the effect of varying m for both Δ_m and Δ_c fixed. The results are shown in Fig.3(**c**)-(**d**). In this situation, we have the presence of the gap as a consequence of m. However no significant change is observed in the lineshape, for both symmetries. Note that, since the space groups Nos 126 and 128 are subgroups of the No 123, the coexistence between the parameter m with a non zero Δ_m or Δ_c still corresponds to those particular groups.

At this point, we would like to make a connection between our theoretical results and the hidden order (HO)

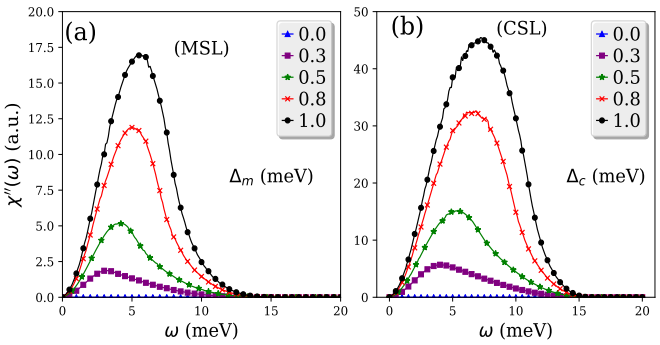

FIG. 2. The Raman response corresponding to A_{2g} symmetry. Figures **(a)** display the Raman signal when we increase the values of Δ_m, while in (**b**) we vary the Δ_c parameter. No gap is observed even though the intensity of the signal is increased when the δ's are increased. No signal is observed when $\Delta_c = \Delta_m = 0$. We set $t_1 = 1.0\ meV$ and use once again a small scattering rate $\delta = 0.035 meV$.

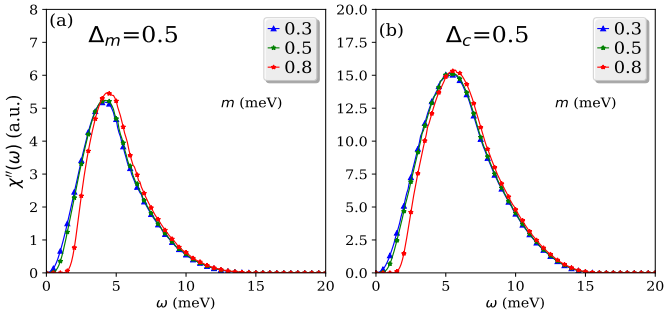

FIG. 3. The Raman response for A_{2g} symmetry when we have the presence of m. In (**a**), we have the modulated SL phase, which corresponds to state No 126. while (**b**) displays the spectra for the chiral SL phase, which corresponds to lattice symmetry No 128. The presence of m is signalized by a gap opening in both phases.

phase in URu_2Si_2. Despite almost forty years of investigation, the nature of this mysterious phase remains a puzzle. A vast arsenal of experimental techniques have been employed over the years to investigate the HO phase (for a recent review see [21, 22]), and, more recently, the Raman scattering [7, 8, 23, 24] should be included in this list. The results from Raman provided new experimental constraints for the theoretical propositions to explain the HO. We briefly summarize some of these results.

The first studies have evidenced that the HO phase presents a sharp excitation at 1.7 meV and a gap in the electronic continuum below 6.8 meV. These signatures have only a A_{2g} symmetry [7, 8]. On top of that, the study in [8] also reported a peak in A_{1g}. The Raman spectra present signatures (of the A_{1g} and A_{2g} symmetries) in the HO phase. They interpret that the symmetry broken by the HO parameter results in crystal field states with distinct chiral properties. They defined this ordering as being a commensurate hexadecapolar order [25].

Our results show that the A_{2g} symmetry displays some signals when one of the two parameters Δ_c or Δ_m of the spin liquid phases are active. Otherwise, no signal is expected. This result opens the possibility for the two spin liquid states: the modulated SL with space symmetry group No 126 ($P4/nnc$) and the chiral SL, with point symmetry space No 128 ($P4/mnc$). It clearly eliminates the purely commensurate LSO state, which does not provide any signal in A_{2g} symmetry. Nevertheless, we cannot distinguish with exactitude which SL phase is more or less the most appropriate because the Raman signatures look the same for the modulated and the chiral SL. Indeed, similarly to what we have found for A_{1g} and B_{2g} symmetries, the chiral SL and the modulated SL become pseudogapped phases when $m = 0$. The gap is uniquely observed only when m is taken into account. Therefore, in order to choose which SL phase is more appropriate to describe the HO, we must also consider other properties, like the point group symmetry, to make more precise predictions about the HO in URu_2Si_2.

In the framework of the cuprates systems [26], the A_{2g} symmetry may account for the appearance of excitations in which quantum fluctuations destroy the Néel order, with the elementary excitations having a fractional character with a chiral nature [12, 27, 28]. This may favor the choice of chiral SL phase as the natural framework for the appearance of such excitations. However, in their analysis, Harima *et al* [18] suggested that the space group No 128 might be incompatible with some nuclear resonance experiments on URu_2Si_2. On the other side, space group No 128 is compatible with the commensurate chirality density wave state discussed in ref.[8].

IV. THE RAMAN RESPONSE FOR A_{1g} AND B_{2g} SYMMETRIES

A. The effective density response

As a complement to the analysis in the A_{2g} symmetry, we shall discuss the signatures in other irreducible symmetries of the D_{4h} point group, i.e., A_{1g}, B_{1g} and B_{2g}. Even if there is no experimental indication of B_{1g} and B_{2g} at the HO state, our discussion here may cover, in a general manner, systems with BCT lattice structure. We calculate the Raman response by employing the effective density-density correlation function. For this purpose, we consider the limit of small momentum transfer, which allows us to use the standard effective mass approximation to calculate the appropriate Raman vertex for each particular symmetry.

The physical quantity observed experimentally is the Raman scattering cross-section. This quantity is determined by the dynamical structure factor $\tilde{S}(\mathbf{q}, i\omega)$, which is directly related to the imaginary part of the Raman

response $\tilde{\chi}$ through the fluctuation-dissipation theorem

$$\tilde{S}^{\lambda}(\mathbf{q},\omega) = -\frac{1}{\pi}[1+n_B(\omega)]\mathrm{Im}[\tilde{\chi}^{\lambda}(\mathbf{q},\omega)]. \quad (16)$$

In this equation, $n_B(\omega)$ is the Bose distribution function and λ stands for the particular symmetry of the Raman excitation. The Raman response measures the "effective density" fluctuations produced by the density-density correlation function

$$\tilde{\chi}^{\lambda}(\mathbf{q},i\omega_n) = -\frac{1}{\mathcal{V}}\int_0^{\beta} d\tau e^{i\omega_n\tau}\langle T_{\tau}(\tilde{\rho}^{\lambda}(\mathbf{q},\tau)\tilde{\rho}^{\lambda}(-\mathbf{q},0))\rangle, \quad (17)$$

where $\tilde{\rho}^{\lambda}$ is the effective density operator. The effective polarization-dependent density operator [2] is written as

$$\hat{\tilde{\rho}}^{\lambda}(\mathbf{q},\tau) = \sum_{\mathbf{k}} \Psi^{\dagger}_{\mathbf{k}+\mathbf{q}/2}(\tau)\boldsymbol{\gamma}^{\lambda}(\mathbf{k})\Psi_{\mathbf{k}-\mathbf{q}/2}(\tau) \quad (18)$$

where $\gamma^{\lambda}(\mathbf{k})$ is the matrix which originate from the second derivatives of $h_{\mathbf{k}}$. Then, it follows that the density-density correlation function can be written as

$$\tilde{\chi}^{\lambda}(i\omega_n) = \frac{1}{\beta\mathcal{V}}\sum_{\mathbf{k},\nu_{n'}} \mathrm{Tr}[\gamma^{\lambda}(\mathbf{k})G_{\mathbf{k}}(i\nu_{n'}+i\omega_n)\gamma^{\lambda}(\mathbf{k})G_{\mathbf{k}}(i\nu_{n'})]. \quad (19)$$

All the analytical steps to develop this correlation function follows what we have done in the previous section for the analysis of the A_{2g} symmetry. For each one of the irreducible representations we have to write an appropriate vertex which corresponds to each of these symmetries. If we consider the effective mass approximation limit, with $\mathbf{q}\to 0$, these vertices are defined simply as

$$\boldsymbol{\gamma}^{A_{1g}}(\mathbf{k}) = \frac{\partial^2 h_{\mathbf{k}}}{\partial k_x^2} + \frac{\partial^2 h_{\mathbf{k}}}{\partial k_y^2}, \quad (20)$$

$$\boldsymbol{\gamma}^{B_{1g}}(\mathbf{k}) = \frac{\partial^2 h_{\mathbf{k}}}{\partial k_x^2} - \frac{\partial^2 h_{\mathbf{k}}}{\partial k_y^2}, \quad (21)$$

$$\boldsymbol{\gamma}^{A_{2g}}(\mathbf{k}) = \frac{\partial^2 h_{\mathbf{k}}}{\partial k_x \partial k_y} - \frac{\partial^2 h_{\mathbf{k}}}{\partial k_y \partial k_x}. \quad (22)$$

$$\boldsymbol{\gamma}^{B_{2g}}(\mathbf{k}) = \frac{\partial^2 h_{\mathbf{k}}}{\partial k_x \partial k_y} + \frac{\partial^2 h_{\mathbf{k}}}{\partial k_y \partial k_x}. \quad (23)$$

Next, with that in hand, we shall present the numerical evaluation of Eq.(19). We note that, for our model, it is not possible to obtain results for the B_{1g} symmetry and, indeed, with the effective mass approximation, the vertex for A_{2g} symmetry vanishes identically.

B. Numerical results

Our numerical analysis follows the same procedure done in the previous section, but now, we use the correlation functions in Eq.(19) and extract its imaginary part as the Raman spectra. We calculated all the results in the limit of $T\to 0$. We concentrate on the response provided by A_{1g} and B_{2g}, since the B_{1g}, in this case, does not provide any Raman signature. We do not observe any Raman signal for the general PM phase associated with the space group No 139. This typical phase has the space group associated with the full BCT lattice. We observe some signal if only one of the parameters that break the lattice translation symmetry is activated.

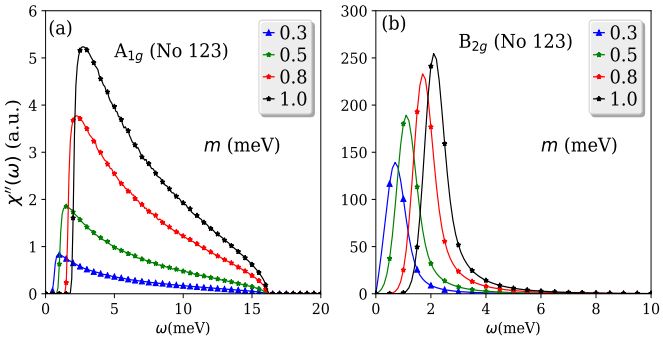

FIG. 4. The Raman signals for the A_{1g} ((**a**)) and B_{2g} symmetries ((**b**)) in the state No 123, characterized by m parameter. In both cases, we clearly see the presence of the gap for different values of m. In this analysis, we use of $t_1 = 1.0\ meV$ and small phenomenological scattering rate $\delta = 0.035\ meV$ in the imaginary part of the self-energy in the Green's function.

In Fig.4 we present the results concerning the A_{1g} and B_{2g} symmetries. In this analysis, we keep only the hopping t_1 active while varying the parameters that specify each space group with lower symmetry. In this particular case, we test the variation of m describing the state No 123. Fig.4(**a**) shows the Raman spectra for the A_{1g} symmetry. We vary the values of m and observe the presence of a gap followed by an electronic continuum. The signal vanishes for values of $\omega \approx 15.5\ meV$, and the gap widens when we increase the values of m. In Fig.4(**b**), we show the spectra for the B_{2g} symmetry case. We also observe the presence of the gap, but the signal features a quasielastic response, analogous to the ones predicted theoretically in ref.[29] for iron systems.

Fig.5 displays the responses for the spin liquids states. The state No 126, which is characterized by the Δ_m parameter, denotes the MSL phase. Their Raman response for A_{1g} and B_{2g} are shown in Fig.5(**a-b**), respectively. In both symmetries, there is no presence of the gap. For A_{1g} the lineshape characterizes itself by a quasielastic narrow peak followed by an electronic continuum that spreads up and moves progressively to high energy when we increase the values of Δ_m. In the B_{2g} symmetry, the spectra display a quasielastic broad peak for a small $\Delta_m = 0.3\ meV$ and transform themselves into a electronic continuum for large values of Δ_m.

Fig.5-(**c**)-(**d**) show the Raman signals for the state No 128, the CSL which is characterized by Δ_c parameter. Once again there is no presence of gap for the A_{1g} and B_{2g} symmetries. For the A_{1g} case, the spectra distinguish themselves by a quasielastic response with a narrow peak which is followed by a small electronic continuum. The

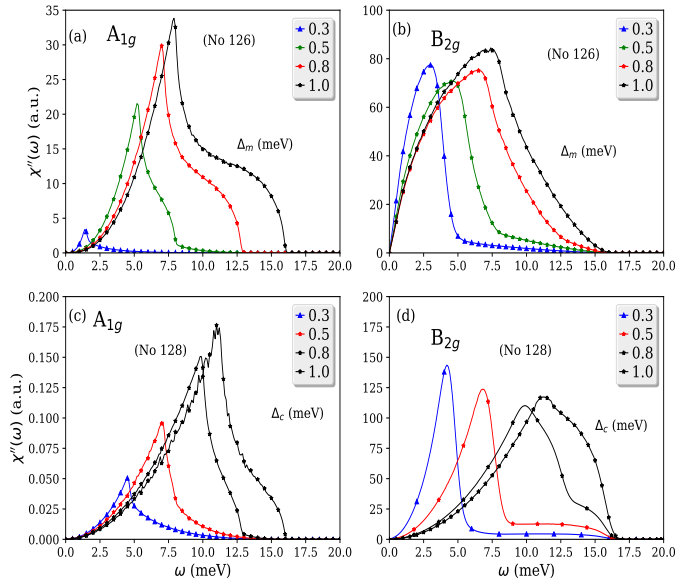

FIG. 5. The Raman spectra for the A_{1g} and B_{2g} symmetries. Figure **(a)-(b)** show our results for the modulated SL phase (space group No 126) at A_{1g} and B_{2g} respectively. In contrast, (**(c)-(d)**) show the responses for the chiral SL phase (space group No 128). For this analysis, we use the values of $t_1 = 1.0\ meV$ and small phenomenological scattering rate $\delta = 0.035\ meV$ in the imaginary part of the self-energy in the Green's function.

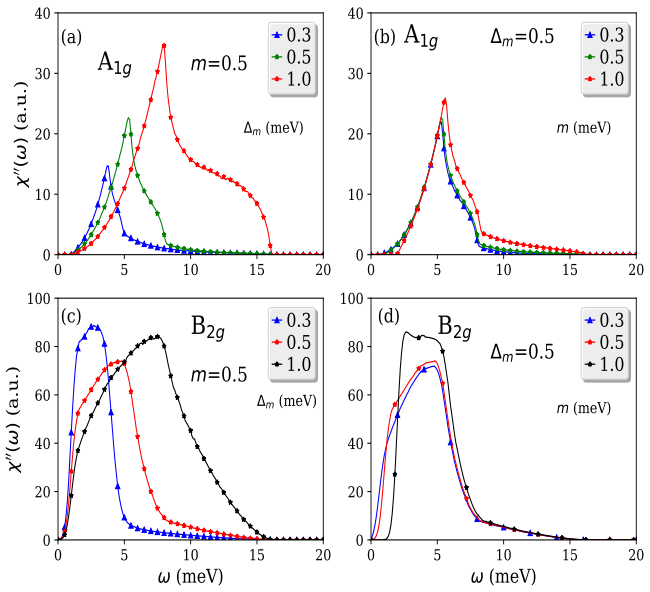

FIG. 6. The Raman spectra for A_{1g} and B_{2g} symmetries when we keep m together with the Δ_m, the MSL parameter (space group No 126). In (**a**)-(**c**), we display the Raman signals for m fixed in the A_{1g} and B_{2g} symmetries, respectively. In (**b-d**), we fixed the value of Δ_m while vary the m parameter. The description of the spectra is discussed further on the text.

electronic continuum does not spread up by increasing the values of Δ_c and seems to be suppressed by large values of this parameter, in contrast to what happened in the modulated spin liquid case. In the B_{2g} symmetry, we observe the evolution of a quasielastic response to a structureless curve by increasing the magnitude of Δ_c. Afterwards, we look at the cases when we have m activated together with the parameters that discriminate the spin liquid phases. Our results are shown in Fig.6 and Fig.7.

In Fig.6, we activate the parameter m and observe its effect in the presence of Δ_m. In Fig.6(**a**)-(**c**), we set a fixed value of $m = 0.5\ meV$ while varying Δ_m. In the A_{1g} symmetry, we observe the presence of the gap followed by a quasielastic peak which increases by increasing the value of Δ_m. Further, we have the presence of an electronic continuum that becomes more robust as we increase Δ_m and moves progressively to high energies as we increase the value of Δ_m. In Fig.6(**c**), we also set the same value of $m = 0.5\ meV$ as we vary the Δ_m in the B_{2g} symmetry. We observe the evolution of the signal by increasing the value of Δ_m. In all cases, it features the presence of the gap but is starting from a quasielastic broad peak and goes to a electronic continuum. In Fig.6(**b**)-(**d**), we fix the value of $\Delta_m = 0.5\ meV$, while varying m. Although the spectra of A_{1g} and B_{2g} are in contrast with each other, in both cases, we can observe the presence of a gap which widens as we increase

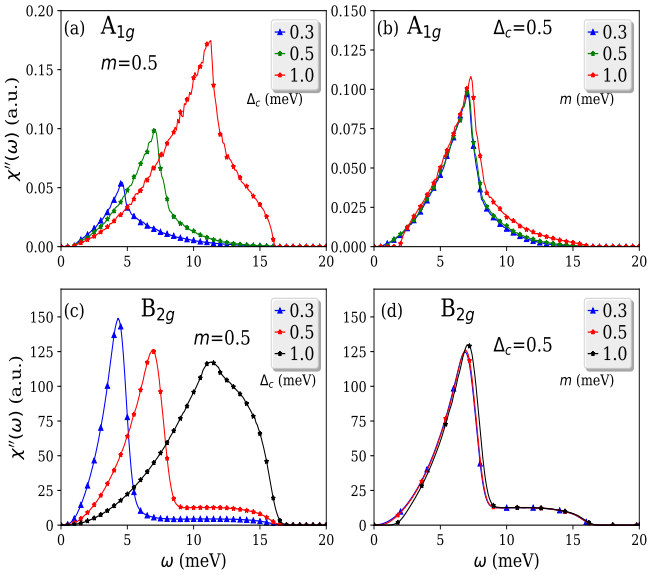

FIG. 7. The Raman spectra for A_{1g} and B_{2g} symmetries for non-zero m and the Δ_c SL parameter (space group No128). In (**a-c**), we display the Raman signals for m fixed in the A_{1g} and B_{2g} symmetries, respectively. In (**b-d**), we fix the value of Δ_c while varying the m parameter. See the text more comments.

the value of m, suggesting that the parameter m is the responsible for its appearance.

The results showed in Fig.7 display the spectra for A_{1g} and B_{2g} symmetries in the chiral SL phase. In Fig.7(**a**)-(**c**), we show the Raman signals when we fix the value of m parameter while varying Δ_c. We can observe the presence of a gap when $m \neq 0$ for both symmetries. For A_{1g} symmetry, Fig.7(**a**), the curve moves progressively along the frequency axis when we increase the value of Δ_c. The line shape exhibits a quasielastic peak and a small electronic continuum. The electronic continuum appears to be suppressed, by increasing Δ_c and then turn the response into a quasielastic peak. For the B_{2g} symmetry, as shown in Fig.7(**c**), when we increase the values of Δ_c, the signal evolves from a quasielastic response to a broad and structureless spectrum. In Fig.7(**b**)-(**d**), we fix the value of Δ_c while varying m for A_{1g} and B_{2g}, respectively. In both cases, the lineshapes of the spectra are not drastically altered, but we see the presence of the gap and its enlargement by the increase of the m parameter.

With this extensive analysis, we can predict that the electronic Raman signal will display clear signatures of the opening of a gap which is a consequence of m parameter. In the case when either Δ_m or Δ_c is activated and keeping $m = 0$, the gap does not manifest itself. Since we consider only the presence of t_1 in all of the analysis of the spectra, the phases exhibit the nesting condition $\varepsilon_{\mathbf{k}\pm\mathbf{Q}} = -\varepsilon_{\mathbf{k}}$. The perfect nesting condition manifests itself when the system is unstable against the short wavelength order, like spin (charge) density-wave or the formation of particle pairs in the superconducting case. In this framework we conclude that the commensurate LSO parameter m is the main responsible for this instability that gives rise to the gap in the Raman spectrum. We are aware that no gap is observed experimentally in URu_2Si_2 for neither A_{1g} nor B_{2g} symmetry. Our interpretation is that, in a multiband system like URu_2Si_2, some electronic continuum in these symmetries is also provided from weakly correlated charge degrees of freedom that are not taken into account in the effective model Hamiltonian studied here. The situation is different with A_{2g} because these "light electrons" are simply not active in such a symmetry.

V. DISCUSSIONS AND CONCLUSIONS

The main conclusive result concerning our Raman responses is the appearance of a gap that manifests itself for the specific A_{1g} and B_{2g} symmetries. We have shown that this gap is a consequence of the commensurate LSO discriminated specifically by the m parameter. Similar responses were observed by Raman scattering in the iron-based superconductor materials [4], though this time for different symmetries (B_{1g} and B_{2g}). The spectra of these materials display many spin-density-wave gaps as expected in a band-folding itinerant picture of multiband systems.

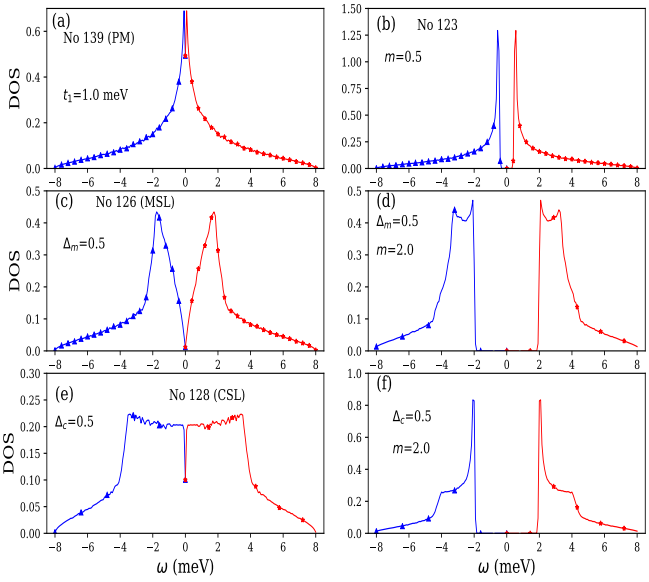

FIG. 8. The density of states (DOS) for the various phases considered in our model. We set the Fermi level E_0 at zero and keep t_1 activated in all phases.

Why does not this gap manifest in the other states that break the lattice translation symmetry? In fact, the answers is that rather than a real gap, what we have is a pseudogap that it is reminiscent from the SL phases. We can confirm this fact by computing the density of states (DOS) $\rho(\omega) = \sum_{\mathbf{k}} \delta(\omega - E^{\pm}_{\mathbf{k}})$. In Fig.8, we plot the DOS for the various phases considered here. In Fig.8(**a**), we show the DOS for the PM state. For a homogeneous hopping t_1, the DOS has singularities at $\omega = -8t_1\ meV$, $\omega = 8t_1\ meV$ and at $\omega = 0$. In Fig.8(**b**), we observe the evolution from the previous plot when we activate m. The singularity now is placed at $\omega = 0.5\ meV$, which corresponds to the values that we set for m. We see clearly the presence of a small gap of twice the order of magnitude of this m parameter. For the two purely SL phases Fig.8(**c**) and Fig.8(**e**), the two bands touch each other when $\omega = 0$. In the modulated SL, it vanishes for $\omega = 0$ while in the chiral SL it is finite at $\omega = 0$. Then, when we turn m on Fig.8(**d**) and Fig.8(**f**), we observe the presence of the gap again (we have extrapolated the value of m to see if the gap is proportional to its value). Another important result is the fact that only band folding with $m \neq 0$ is not sufficient for obtaining a signal in A_{2g}. To pick up signal the in the A_{2g}, it is also required the presence of an SL order term, i.e., at least Δ_m or Δ_c should be different from zero. Unfortunately, our non-interacting model is not able to reproduce the quasielastic peak placed inside the gap, which requires considering more effects due to interactions.

In summary, we proposed an effective model to describe Raman scattering experiments in systems that display the BCT lattice. We have in mind the perspective of stabilizing two different spin liquid states. They are

the modulated SL and the chiral SL phases. Concerning the experimental evidence that is well established with Raman scattering response namely the A_{2g} symmetry in the HO phase, we found that both SL phases present similar Raman responses. In particular, these responses show gapped but non-zero electronic continuum in A_{2g} even at the non-interacting level. The gap is open by the local staggered m parameter, but the A_{2g} continuum is activated by either a chiral SL or a modulated SL order. To select the best candidate to explain the hidden order phase, since both spin liquids give very similar responses, we consider the fact that the existence of time-reversal symmetry breaking in the HO phase remains controversial [30–32]. If we assume that the HO does not break this symmetry, we pick out the modulated SL as the plausible candidate for this non-conventional phase. There is also the possibility of analyzing the A_{2g} signal by applying pressure. In this case, a full track of the A_{2g} signal could be obtained from the HO to the AF phase. Thereby, we could expect that the Raman signatures under applied pressure might predict to be those of the state 123. This means that we predict, in the AF phase a vanishing (or a strong decay) of the electronic continuum in the A_{2g} symmetry.

ACKNOWLEDGMENTS

The authors wish to thank to I. Paul, M.-A Méasson, S. Magalhães, J. Buhot, R. G. Pereira, V. S. de Carvalho, H. Harima, C. Pépin, C. Lacroix and D. Baeriswyl for fruitful discussions. This work was conducted during a scholarship supported by the International Cooperation Program CAPES/COFECUB at the University of Bordeaux. Financed by CAPES – Brazilian Federal Agency for Support and Evaluation of Graduate Education within the Ministry of Education of Brazil. C. F also acknowledges the financial support from CNPq. This work was partially supported by the ANR-DFG grant "Fermi-NESt".

Appendix A: Deriving the dispersion relations

The purpose of this appendix is to clarify the derivations of the relations that were presented in the section II. More precisely the two structure factors $f_m(\mathbf{k})$ and $f_c(\mathbf{k})$, associated with the modulated SL and chiral SL, respectively. We take the Hamiltonian in Eq.(1)

$$H = \sum_i (E_o + m e^{i\mathbf{Q}\cdot\mathbf{R}_i}) c_i^\dagger c_i + \sum_{\langle i,j\rangle} t_{ij} c_i^\dagger c_j. \tag{A1}$$

The sum in sites are related with the BCT lattice. The Hamiltonian can be seen as a sum $H = H_0 + H_t$, where $H_0 = \sum_i (E_o + m e^{i\mathbf{Q}\cdot\mathbf{R}_i}) c_i^\dagger c_i$ and $H_t = \sum_{\langle i,j\rangle} t_{ij} c_i^\dagger c_j$. Let us concentrate on the hopping term

$$H_t = \sum_{\langle i,j\rangle} t_{ij} c_i^\dagger c_j. \tag{A2}$$

We developed the calculation for a general hopping $t_{i,j}$ and at the end we will concentrate only in the first neighbors inter-plane, since the in-plane relations can be derived in the same fashion as for square lattice. For the hopping inter-plane, we have

$$t_{ij} = t_1 \pm i\Delta_c, \tag{A3}$$

and

$$t_{ij} = t_1 \pm \Delta_M. \tag{A4}$$

The sign plus or minus take into account the kind of link between two sites, as explained in section II.

By using the Fourier transform in Eq.(2), we rewrite the Hamiltonian and we end up with

$$H = \frac{1}{N} \sum_{\mathbf{k},\mathbf{k}'} c_{\mathbf{k}}^\dagger c_{\mathbf{k}'} \sum_i e^{-i(\mathbf{k}-\mathbf{k}')\cdot\mathbf{R_i}} E_{\mathbf{R}_i}(\mathbf{k}'), \tag{A5}$$

where we defined $E_{\mathbf{R}_i}(\mathbf{k}') = \sum_\delta t_{i,i+\delta} e^{i\mathbf{k}'\cdot\boldsymbol{\delta}}$ and have considered $j = i + \delta$, with δ being a first neighbor vector. The sum in $\mathbf{k}$ runs over the first Brillouin zone of BCT. The next step is to split the sum in the BCT-Brillouin zone as being a sum of two tetragonal lattices, where we assumed that the BCT is bipartite in two sub-lattices A and B. We end up with four terms

$$\begin{aligned} H = & \frac{1}{N} \sum_{\mathbf{k},\mathbf{k}'} c_{\mathbf{k}}^\dagger c_{\mathbf{k}'} \sum_i e^{-i(\mathbf{k}-\mathbf{k}')\cdot\mathbf{R}_i} E_{\mathbf{R}_i}(\mathbf{k}') \\ & + \frac{1}{N} \sum_{\mathbf{k},\mathbf{k}'} c_{\mathbf{k}}^\dagger c_{\mathbf{k}'} \sum_i e^{-i(\mathbf{k}-\mathbf{k}')\cdot\mathbf{R_i}} E_{\mathbf{R}_i}(\mathbf{k}'+\mathbf{Q}) \\ & + \frac{1}{N} \sum_{\mathbf{k},\mathbf{k}'} c_{\mathbf{k}+\mathbf{Q}}^\dagger c_{\mathbf{k}'} \sum_i e^{-i(\mathbf{k}+\mathbf{Q}-\mathbf{k}')\cdot\mathbf{R}_i} E_{\mathbf{R}_i}(\mathbf{k}') \\ & + \frac{1}{N} \sum_{\mathbf{k},\mathbf{k}'} c_{\mathbf{k}}^\dagger c_{\mathbf{k}+\mathbf{Q}} \sum_i e^{-i(\mathbf{k}-\mathbf{Q}-\mathbf{k}')\cdot\mathbf{R}_i} E_{\mathbf{R}_i}(\mathbf{k}'+\mathbf{Q}). \end{aligned} \tag{A6}$$

Now the sums in $\mathbf{k}$ run over the T-lattice. But the sums in i run over the BCT lattice.

We can also split the sum in the BCT-Lattice in a sum for sub-lattice A and B. This requires that $t_{i,i+\delta} = t_\delta^A$ if $\mathbf{R}_i \in$ A or $t_{i,i+\delta} = t_\delta^B$ if $\mathbf{R}_i \in$ B. The condition $t_\delta^B = \left(t_\delta^A\right)^*$ preserves the hermiticity of the Hamiltonian, which give us the relation between $E_B(\mathbf{k}') = (E_A(\mathbf{k}'))^*$. We know that $\frac{1}{N}\sum_{\mathbf{R}_i} e^{-i(\mathbf{k}-\mathbf{k}')\cdot\mathbf{R}_i} = \frac{1}{2}\delta_{\mathbf{k}\mathbf{k}'}$ and $e^{-i\mathbf{Q}\cdot\mathbf{R}_i} = \pm 1$ if $\mathbf{R}_i$ belongs to A or B, respectively. Then,

$$\begin{aligned} H \; = \; & \frac{1}{2} \sum_{\mathbf{k}} c_{\mathbf{k}}^\dagger c_{\mathbf{k}} [E(\mathbf{k}) + E^*(\mathbf{k})] \\ & + \frac{1}{2} \sum_{\mathbf{k}} c_{\mathbf{k}+\mathbf{Q}}^\dagger c_{\mathbf{k}+\mathbf{Q}} \left[E\left(\mathbf{k}+\mathbf{Q}\right) + E^*\left(\mathbf{k}+\mathbf{Q}\right)\right] \\ & + \frac{1}{2} \sum_{\mathbf{k}} c_{\mathbf{k}+\mathbf{Q}}^\dagger c_{\mathbf{k}} \left[E\left(\mathbf{k}\right) - E^*\left(\mathbf{k}\right)\right] \\ & + \frac{1}{2} \sum_{\mathbf{k}} c_{\mathbf{k}}^\dagger c_{\mathbf{k}+\mathbf{Q}} [E\left(\mathbf{k}+\mathbf{Q}\right) - E^*\left(\mathbf{k}+\mathbf{Q}\right)]. \end{aligned} \tag{A7}$$

We can write the Hamiltonian in a matrix representation, as follows

$$H = \sum_{\mathbf{k}} \Psi^{\dagger}_{\mathbf{k}} h'_{\mathbf{k}} \Psi_{\mathbf{k}}, \tag{A8}$$

with the definition of $\Psi_{\mathbf{k}} = (c_{\mathbf{k}}, c_{\mathbf{k+Q}})^t$ and

$$h'_{\mathbf{k}} = \begin{pmatrix} \frac{E(\mathbf{k})+E^*(\mathbf{k})}{2} & \frac{E(\mathbf{k+Q})-E^*(\mathbf{k+Q})}{2} \\ \frac{E(\mathbf{k})-E^*(\mathbf{k})}{2} & \frac{E(\mathbf{k+Q})+E^*(\mathbf{k+Q})}{2} \end{pmatrix}. \tag{A9}$$

By taking the definition of $E(\mathbf{k})$, the hopping $t_{i,j}$ and considering the wave vector $\mathbf{Q} = \{1,1,1\}$, we can recognize the following terms when doing the sum in the δ neighbors vectors

$$\frac{E(\mathbf{k}) + E^*(\mathbf{k})}{2} = t_1\gamma^1_k + t_2\gamma^2_k + t_3\gamma^3_k, \tag{A10}$$

$$\frac{E\left(\mathbf{k}+\mathbf{Q}\right) + E^*\left(\mathbf{k}+\mathbf{Q}\right)}{2} = -t_1\gamma^1_k + t_2\gamma^2_k + t_3\gamma^3_k, \tag{A11}$$

$$\frac{E\left(\mathbf{k}+\mathbf{Q}\right) - E^*\left(\mathbf{k}+\mathbf{Q}\right)}{2} = \pm i8\Delta_{sl}\gamma^{sl}_k, \tag{A12}$$

$$\frac{E(\mathbf{k}) - E^*(\mathbf{k})}{2} = \mp i8\Delta_{sl}\gamma^{sl}_k. \tag{A13}$$

If we add the contribution from m and E_0 we recover the $h_{\mathbf{k}}$ matrix in Eq.(4) defined in section II.

We would like to highlight the derivation of the $\mathbf{k}$ dependence in $V_{\mathbf{k}}$, which came from the Δ's in $t_{i,j}$. We take the first neighbors inter-plane. In this case, the sum in δ take in to account the eight different neighbors interplane on the BCT lattice. They are listed in the table (II) and represented in the Fig.9. The first sum in δ taking the t_1 term produce the γ^1_k and the second sum give us $f_{SL}(\mathbf{k})$. This last terms can be $f_m(\mathbf{c})$ or $f_m(\mathbf{k})$ depending on the definition of t_{ij}. This complete our demonstration of the relation that have been presented so far in that section.

TABLE II. the eight first neighbours interplane for the BCT lattice.

δ_i	(x,y,z)
δ_1	$(a/2, a/2, c/2)$
δ_2	$(-a/2, a/2, c/2)$
δ_3	$(-a/2, -a/2, c/2)$
δ_4	$(a/2, -a/2, c/2)$
δ_5	$(-a/2, -a/2, -c/2)$
δ_6	$(a/2, -a/2, -c/2)$
δ_7	$(a/2, a/2, -c/2)$
δ_8	$(-a/2, a/2, -a/2)$

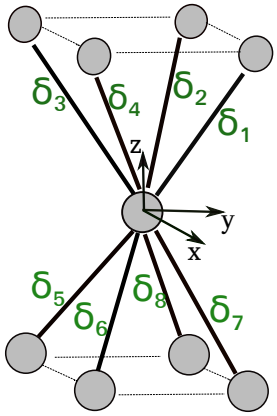

FIG. 9. The BCT lattice with its eight first neighbors interplane. The values of each unitary vector are listed in table (II) bellow.

Appendix B: Extracting the A_{2g} response

We shall show now how to extract a non-zero signal for the symmetry A_{2g}. Consider the expression for the vertex for A_{2g} defined in section III, as

$$\tilde{\gamma}^{A_{2g}}(\mathbf{k}) = \frac{\partial h_{\mathbf{k}}}{\partial k_x}\frac{\partial h_{\mathbf{k}}}{\partial k_y} - \frac{\partial h_{\mathbf{k}}}{\partial k_y}\frac{\partial h_{\mathbf{k}}}{\partial k_x}. \tag{B1}$$

This is analogous to the commutation

$$\tilde{\gamma}^{A_{2g}}(\mathbf{k}) = \left[\frac{\partial h_{\mathbf{k}}}{\partial k_x}, \frac{\partial h_{\mathbf{k}}}{\partial k_y}\right]. \tag{B2}$$

We can make use of the Pauli matrices together with an identity, and rewrite $h_{\mathbf{k}}$ as

$$h_{\mathbf{k}} = A_{\mathbf{k}}\mathbf{1} + \mathbf{Re}(V_{\mathbf{k}})\boldsymbol{\sigma}_1 + \mathbf{Im}(V_{\mathbf{k}})\boldsymbol{\sigma}_2 + B_{\mathbf{k}}\boldsymbol{\sigma}_3, \tag{B3}$$

with

$$A_{\mathbf{k}} = \frac{\epsilon_{\mathbf{k}} + \epsilon_{\mathbf{k+Q}}}{2}, \tag{B4}$$

$$B_{\mathbf{k}} = \frac{\epsilon_{\mathbf{k}} - \epsilon_{\mathbf{k+Q}}}{2}. \tag{B5}$$

By using the notation, $\mathrm{Im}(V_{\mathbf{k}}) = V''_{\mathbf{k}}$ and $\mathrm{Re}(V_{\mathbf{k}}) = V'_{\mathbf{k}}$, the commutator can be written as

$$\begin{aligned}\left[\frac{\partial h_{\mathbf{k}}}{\partial k_x}, \frac{\partial h_{\mathbf{k}}}{\partial k_y}\right] &= \left(\frac{\partial V'_{\mathbf{k}}}{\partial k_x}\frac{\partial V''_{\mathbf{k}}}{\partial k_y} - \frac{\partial V''_{\mathbf{k}}}{\partial k_x}\frac{\partial V'_{\mathbf{k}}}{\partial k_y}\right)[\boldsymbol{\sigma}_1, \boldsymbol{\sigma}_2] \\ &+ \left(\frac{\partial V''_{\mathbf{k}}}{\partial k_x}\frac{\partial B_{\mathbf{k}}}{\partial k_y} - \frac{\partial B_{\mathbf{k}}}{\partial k_x}\frac{\partial V''_{\mathbf{k}}}{\partial k_y}\right)[\boldsymbol{\sigma}_2, \boldsymbol{\sigma}_3] \\ &+ \left(\frac{\partial B_{\mathbf{k}}}{\partial k_x}\frac{\partial V'_{\mathbf{k}}}{\partial k_y} - \frac{\partial V'_{\mathbf{k}}}{\partial k_x}\frac{\partial B_{\mathbf{k}}}{\partial k_y}\right)[\boldsymbol{\sigma}_3, \boldsymbol{\sigma}_1]\end{aligned} \tag{B6}$$

By using the commutation relations for the Pauli matrices, we have

$$\begin{aligned}\left[\frac{\partial E_{\mathbf{k}}}{\partial k_x}, \frac{\partial E_{\mathbf{k}}}{\partial k_y}\right] &= \left(\frac{\partial V''_{\mathbf{k}}}{\partial k_x}\frac{\partial B_{\mathbf{k}}}{\partial k_y} - \frac{\partial B_{\mathbf{k}}}{\partial k_x}\frac{\partial V''_{\mathbf{k}}}{\partial k_y}\right)2i\boldsymbol{\sigma}_1 \\ &+ \left(\frac{\partial B_{\mathbf{k}}}{\partial k_x}\frac{\partial V'_{\mathbf{k}}}{\partial k_y} - \frac{\partial V'_{\mathbf{k}}}{\partial k_x}\frac{\partial B_{\mathbf{k}}}{\partial k_y}\right)2i\boldsymbol{\sigma}_2 \\ &+ \left(\frac{\partial V'_{\mathbf{k}}}{\partial k_x}\frac{\partial V''_{\mathbf{k}}}{\partial k_y} - \frac{\partial V''_{\mathbf{k}}}{\partial k_x}\frac{\partial V'_{\mathbf{k}}}{\partial k_y}\right)2i\boldsymbol{\sigma}_3.\end{aligned} \tag{B7}$$

In our model, we have explicitly defined the form of $V_{\mathbf{k}}$. By doing so, all the terms that involve derivatives with respect to its real part are identically vanishing. The only term that survives is the fist one on the right hand side. Therefore, we have that

$$\tilde{\gamma}^{A_{2g}}(\mathbf{k}) = \left(\frac{\partial V''_{\mathbf{k}}}{\partial k_x}\frac{\partial B_{\mathbf{k}}}{\partial k_y} - \frac{\partial V''_{\mathbf{k}}}{\partial k_y}\frac{\partial B_{\mathbf{k}}}{\partial k_x}\right) 2i\boldsymbol{\sigma}_1. \quad \text{(B8)}$$

From this result, we can check if the $\gamma^{A_{2g}}(\mathbf{k})$ is invariant under time reversal symmetry or not. For spinless particles, the time reversal operator T is directly connected to the complex conjugation operator K, i.e., $T = K$. If a particular operator is invariant under time reversal symmetry, this means that

$$T\hat{A}T^{-1} = \hat{A}. \quad \text{(B9)}$$

For our operator $\gamma^{A_{2g}}(\mathbf{k})$ It follows that

$$T\tilde{\gamma}^{A_{2g}}(\mathbf{k})T^{-1} = -\left(\frac{\partial V''_k}{\partial k_x}\frac{\partial B_k}{\partial k_y} - \frac{\partial V''_k}{\partial k_y}\frac{\partial B_k}{\partial k_x}\right) 2i\boldsymbol{\sigma}_1 \quad \text{(B10)}$$

However, time reversal operation also changes momentum from $\mathbf{k} \to -\mathbf{k}$. Here we keep in mind the definitions of $B_{\mathbf{k}}$ in Eq.(B5) and $V_{\mathbf{k}} = m + i\Delta_{c/m}f_{c/m}(\mathbf{k})$. The function $B_{\mathbf{k}}$ is always even because of the dispersion $\varepsilon_{\mathbf{k}}$. For the imaginary part of $V_{\mathbf{k}}$, we have to consider the two spin liquid dispersions. For the chiral spin liquid $\gamma^c_{\mathbf{k}}$ is even, while for the modulate spin liquid $\gamma^m_{\mathbf{k}}$ is odd. Therefore

$$f_c(-\mathbf{k}) = f_c(\mathbf{k}), \quad \text{(B11)}$$
$$f_m(-\mathbf{k}) = -f_m(\mathbf{k}). \quad \text{(B12)}$$

These results show that, in terms of time reversal symmetry, only the modulated SL has a $\tilde{\gamma}^{A_{2g}}(\mathbf{k})$ time reversal invariant, as it pointed out [16, 33, 34] if the HO does not break this symmetry. In contrast, for the chiral SL, there is a breaking of the time reversal symmetry [27].

[1] B. S. Shastry and B. I. Shraiman, Physical Review Letters **65**, 1068 (1990).
[2] T. P. Devereaux and A. P. Kampf, International Journal of Modern Physics B **11**, 2093 (1997).
[3] T. P. Devereaux and A. P. Kampf, Phys. Rev. B **59**, 6411 (1999).
[4] Y.-X. Yang, Y. Gallais, F. Rullier-Albenque, M.-A. Méasson, M. Cazayous, A. Sacuto, J. Shi, D. Colson, and A. Forget, Phys. Rev. B **89**, 125130 (2014).
[5] Y. Gallais and I. Paul, Comptes Rendus Physique **17**, 113 (2016), iron-based superconductors / Supraconducteurs Ã base de fer.
[6] S. L. Cooper, M. V. Klein, M. B. Maple, and M. S. Torikachvili, Phys. Rev. B **36**, 5743 (1987).
[7] J. Buhot, M.-A. Méasson, Y. Gallais, M. Cazayous, A. Sacuto, G. Lapertot, and D. Aoki, Phys. Rev. Lett. **113**, 266405 (2014).
[8] H.-H. Kung, R. E. Baumbach, E. D. Bauer, V. K. Thorsmølle, W.-L. Zhang, K. Haule, J. A. Mydosh, and G. Blumberg, Science , 1339 (2015).
[9] J. Nasu, J. Knolle, D. L. K. Y. Motome, and R. Moessner, Nature Physics **7** (2016), 10.1038/ncomms12286.
[10] A. Glamazda, P. Lemmens, S. H. Do, Y. S. Choi, and K. Y. Choi, Nature Communications **12**, 912 (2016).
[11] T. P. Devereaux and R. Hackl, Rev. Mod. Phys. **79**, 175 (2007).
[12] D. V. Khveshchenko and P. B. Wiegmann, Phys. Rev. Lett. **73**, 500 (1994).
[13] N. Nagaosa and P. Lee, Phys. Rev. B **43**, 1233 (1991).
[14] P. S. Riseborough, B. Coqblin, and S. G. Magalhães, Phys. Rev. B **85**, 165116 (2012).
[15] P. M. Oppeneer, S. Elgazzar, J. Rusz, Q. Feng, T. Durakiewicz, and J. A. Mydosh, Phys. Rev. B **84**, 241102 (2011).
[16] T. Das, Scientific Reports **2**, 1 (2012).
[17] C. Farias, C. Thomas, C. Pépin, A. Ferraz, C. Lacroix, and S. Burdin, Phys. Rev. B **94**, 134420 (2016).
[18] H. Harima, K. Miyake, and J. Flouquet, Journal of the Physical Society of Japan **79**, 033705 (2010).
[19] C. Pépin, M. R. Norman, S. Burdin, and A. Ferraz, Phys. Rev. Lett. **106**, 106601 (2011).
[20] A. Kitaev, Annals of Physics **321**, 2 (2006), january Special Issue.
[21] J. A. Mydosh and P. M. Oppeneer, Rev. Mod. Phys. **83**, 1301 (2011).
[22] W. Knafo, D. Aoki, G. W. Scheerer, F. Duc, F. Bourdarot, K. Kuwahara, H. Nojiri, L.-P. Regnault, and J. Flouquet, ArXiv e-prints (2017), arXiv:1708.06122 [cond-mat.str-el].
[23] J. Buhot, *Hidden orders and magnetism studied by Raman spectroscopy under extreme conditions*, Theses, Université Paris Diderot-Paris 7 Sorbonne Paris Cité (2015).
[24] J. Buhot, Y. Gallais, M. Cazayous, A. Sacuto, P. Piekarz, G. Lapertot, D. Aoki, and M.-A. Méasson, Physica B: Condensed Matter **506**, 19 (2017).
[25] H. Kusunose and H. Harima, Journal of the Physical Society of Japan **80**, 084702 (2011).
[26] R. Liu, D. Salamon, M. V. Klein, S. L. Cooper, W. C. Lee, S.-W. Cheong, and D. M. Ginsberg, Phys. Rev. Lett. **71**, 3709 (1993).
[27] X. G. Wen, F. Wilczek, and A. Zee, Phys. Rev. B **39**, 11413 (1989).
[28] X.-G. Wen, Phys. Rev. B **65**, 165113 (2002).
[29] Y.-X. Yang, Y. Gallais, F. Rullier-Albenque, M.-A. Méasson, M. Cazayous, A. Sacuto, J. Shi, D. Colson, and A. Forget, Phys. Rev. B **89**, 125130 (2014).
[30] E. R. Schemm, R. E. Baumbach, P. H. Tobash, F. Ronning, E. D. Bauer, and A. Kapitulnik, Phys. Rev. B **91**, 140506 (2015).
[31] I. Kawasaki, I. Watanabe, A. Hillier, and D. Aoki, Jour-

nal of the Physical Society of Japan **83**, 094720 (2014).
[32] T. Shibauchi, H. Ikeda, and Y. Matsuda, Philosophical Magazine **94**, 3747 (2014).
[33] C. Thomas, S. Burdin, C. Pépin, and A. Ferraz, Phys. Rev. B **87**, 014422 (2013).
[34] T. Das, Philosophical Magazine **94**, 3838 (2014).